

An Enzyme-Based Microfluidic Biofuel Cell

Makoto Togo, Hirokazu Kaji, Takashi Abe, and Matsuhiko Nishizawa*

* Professor

Department of Bioengineering and Robotics, Graduate School of Engineering

E-mail: nishizawa@biomems.mech.tohoku.ac.jp



Abstract

Vitamin K₃-modified poly-L-lysine (PLL-VK₃) was synthesized and used as the electron transfer mediator during catalytic oxidation of NADH by diaphorase (Dp) at the anode of biofuel cell. PLL-VK₃ and Dp were co-immobilized on an electrode and then coated with NAD⁺-dependent glucose dehydrogenase (GDH). The resulting enzymatic bilayer (abbreviated PLL-VK₃/Dp/GDH) catalyzed glucose oxidation. Addition of carbon black (Ketjenblack, KB) into the bilayer enlarged the effective surface area of the electrode and consequentially increased the catalytic activity. An oxidation current of ca. 2 mA cm⁻² was observed when the electrochemical cell contained a stirred 30 mM glucose, 1.0 mM NAD⁺, pH 7.0 phosphate-buffered electrolyte solution. The performance of glucose/O₂ biofuel cells, constructed as fluidic chips with controllable fuel flow and containing a KB/PLL-VK₃/Dp/GDH-coated anode and a Ag/AgCl or a polydimethylsiloxane-coated Pt cathode, were evaluated. The open circuit voltage of the cell with the PDMS-coated Pt cathode was 0.55 V and its maximum power density was 32 μW cm⁻² at 0.29 V when a pH 7.0-buffered fuel containing 5.0 mM glucose and 1.0 mM NAD⁺ was introduced into the cell at a flow rate of 1.0 mL min⁻¹. The cell's output increased as the flow rate increased. During 18 hours of continuous operation of the cell with a load of 100 kΩ, the output current density declined by ca.50 %, probably due to swelling of the enzyme bilayer.

1. Introduction

Enzymatic biofuel cells that generate electric power from the oxidation of carbohydrates such as glucose [1-10] or alcohol [11-13] have recently attracted attention because such cells can have a simple structural design (non-compartmentalized) and can operate under mild conditions. The basic characteristics of enzymatic biofuel cells are generally dictated by the enzyme and the electron transfer mediator used [14-16]. Although, based on recent reports, mediator-free electrocatalysis may soon be possible [17,18]. Mediator molecules, when situated at the anode, must have a negative redox potential. They must also be environmentally inert so that they can be easily disposed of (with the spent cell) and/or implanted as part of a medical device without harming the patient. Therefore, 2-methyl-1,4-

naphthoquinone (vitamin K₃, VK₃) is potentially a most promising mediators of diaphorase (Dp), which oxidizes nicotinamide-adenine dinucleotide (NADH) to NAD⁺ [19,20]. NAD⁺ is a cosubstrate for dehydrogenase, which comprise the largest group of redox enzymes known and includes NAD⁺-dependent glucose dehydrogenase (GDH). Sato *et al.* immobilized poly-L-lysine that had been modified with a VK₃ derivative and Dp on an electrode surface. This system exhibits diffusion-controlled NADH oxidation [19]. Recently, we constructed an electrode that could be used for glucose oxidation by coating it with a Dp/GDH enzyme bilayer. The inner Dp layer was co-immobilization with VK₃-modified polyallylamine (PAA) [10].

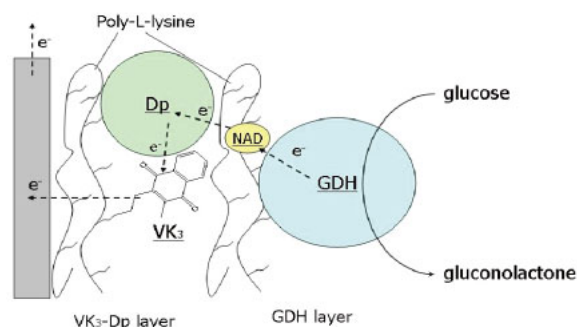


Fig. 1. The presumptive electron-relay/glucose oxidation system catalyzed by PLL-VK₃/Dp/GDH.

The physical design of an enzymatic biofuel cell is an important aspect of biofuel cell research. Since these fuel cells would power independent power-on-chips and micro-electro-mechanical-systems, they must be micro-miniature power sources [14]. Additionally, an implanted device [2-5, 7,14], such as one that regulates blood flow, would need a microfluidic-type biofuel cell as a power source. Therefore advanced microfabrication techniques, such as those used in the construction of primary batteries [21,22], fuel cells [23-25] will also probably be used to build the microfluidic components of enzymatic biofuel cells.

For the work reported herein, we first characterized the VK₃-modified poly-L-lysine (PLL-VK₃) as a mediator of Dp and then tested PLL-VK₃/Dp/GDH bilayer-coated anodes (with and without Ketjenblack

(KB) present) for their abilities to oxidized glucose (presumably in the manner outlined in Fig. 1.) The electrochemical properties of a KB/PLL-VK₃/Dp/GDH-coated anode were evaluated using a conventional electrochemical cell and a microfabricated fluidic cell. The performance and stability of a biofuel cell containing a KB/PLL-VK₃/Dp/GDH-coated anode, a polydimethylsiloxane (PDMS)-coated Pt cathode, and air-saturated glucose fuel were studied at various fuel flow rates.

2. Methods

2.1. Reagents

To synthesize VK₃-modified poly-L-lysine (PLL-VK₃) a procedure similar to one previously described [10] was used. 2-(3-Carboxypropyl)-3-methyl-1,4-naphthoquinone was activated by *N*-hydroxy-succinimide and then reacted with poly-L-lysine hydrochloride (MW ca. 80,000, SIGMA) so as to modify ca. 40 % of the backbone amide nitrogens. The *Bacillus stearothermophilus* diaphorase (EC 1.6.99; 1090 U/mg) was purchased from Unitika. NAD⁺-dependent glucose dehydrogenase (EC 1.1.1.47; 250 U/mg) was donated by TOYOBO. Ketjenblack (EC-600JD) was supplied by Ketjen Black International, Inc. PDMS (SYLPOT 184 W/C) was purchased from Dow Corning Toray. NADH and NAD⁺ were used as received from Oriental Yeast Co.

2.2. Electrodes and electrochemical measurements

Descriptions of the preparations of PLL-VK₃/Dp/GDH-coated electrodes follow. An 8 μL PLL-VK₃ solution (4.83 mM VK₃) was mixed with a 2 μL Dp solution (14 $\mu\text{g } \mu\text{L}^{-1}$ in 50 mM phosphate, pH 7.0). A 4 μL portion of the resulting solution was put onto a glassy carbon (GC) electrode (surface area, 0.07 cm²) and left to dry for 2 h. When KB was to be part of the system, first, 10 μL of the PLL-VK₃/Dp solution (described above) was mixed with 1 μL of KB that was dispersed in water (ca. 13 mg mL⁻¹). Then, a GC electrode was coated with a 4.4 μL portion of this mixture. To create the enzymatic bilayer, the surface of a PLL-VK₃/Dp-coated electrode (with or without KB present) was coated with 4 μL of a solution composed of equal volumes of a 16 $\mu\text{g } \mu\text{L}^{-1}$ GDH, 50 mM phosphate, pH 7.0 solution and a 16 mg mL⁻¹ PLL solution. Because the isoelectric points are 4.7 for Dp, 4.5 for GDH, and 9.74 for lysine, electrostatic interactions between the enzymes and PLL cause an insoluble catalytic bilayer to form at pH 7.0.

The Pt cathode's PDMS coating was constructed by placing a 2 mg mL⁻¹ aqueous PDMS emulsion (Toray Dow Corning Silicone, DC 85 ADDITIVE) onto a Pt plate electrode (66.7 μL of the emulsion per cm²) and then drying the coated electrode for 3 h at room temperature [26].

All electrochemical measurements were performed in 50 mM phosphate, 0.1 M NaCl (pH 7.0) at 37 °C. The electrochemical properties of the two experimental electrodes (with and without KB present) were characterized using a three electrode system (Hokuto Denko HSV-100 electrochemical analyzer) containing an experimentally-modified GC-disc electrode (3 mm in diam.) as the working electrode, an Ag|AgCl (saturated KCl) reference electrode, and a platinum wire counter electrode.

2.3. Microfluidic biofuel cell

To evaluate the performance of the KB/PLL-VK₃/Dp/GDH-coated electrode as an anode of a fuel cell, we constructed microfluidic fuel cells of the type shown in Fig. 2. Electrodes were patterned on the surfaces of glass slides by photolithography and sputtering, which is a lift-off process. The anode's electrode was an enzyme-modified gold disc (2 mm in diam.). The cathode's electrode was either PDMS-coated platinum (3 mm \times 10 mm) or a Ag|AgCl half-cell (2 mm in diam.). The Ag|AgCl cathode was fabricated by coating a Pt disc with Ag|AgCl ink (BAS Inc.) that was then cured at 80 °C for 2 h. The fluidic channel was fabricated from PDMS film. The channel height was 1 mm and its width was 3 mm. The fuel cell performance was evaluated by measuring the cell voltage while varying the external resistance between 1 k Ω and 3 M Ω .

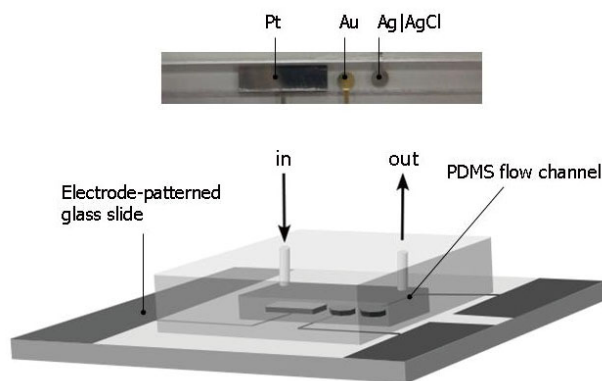


Fig. 2. The structure of the microfluidic biofuel cell used in this study.

3. Results

3.1. Electrochemical properties of the (KB) PLL-VK₃/Dp/GDH-modified electrodes

The PLL-VK₃/Dp/GDH-modified electrode exhibited a reversible voltammetric waves that have the mid-peak potential of -0.27 V which is similar to that found for dissolved aqueous VK₃ (-0.19 V, pH 7.0). The separation between the oxidation and reduction peak potentials is 50 mV, while the separation increases slightly as the scan rate increases. The peak currents increased linearly as the scan rate increases, which is typical for a cell with an electrode that has redox molecules adsorbed on its surface.

As shown in Fig. 4, a catalytic oxidation current appeared on addition of 3.0 mM NADH (Fig. 3b, dashed curve) and was 50 times larger than we reported previously for the PAA-VK₃ system [10]. The longer side chains of PLL should increase the flexibility and the reach of the attached VK₃ molecules, which should, in turn, increase the frequency and productivity of collisions with the redox centers of Dp molecules. When both 3.0 mM glucose and 1.0 mM NAD⁺ were present, glucose-oxidizing catalytic currents resulted (Fig. 3c); the cell's voltammogram was similar to the one obtained when 3.0 mM NADH was present (Fig. 3b), suggesting that the presumptive electron-relay system diagramed in Fig. 1 functioned in the enzyme bilayer. It is worth noting that other NAD⁺-dependent

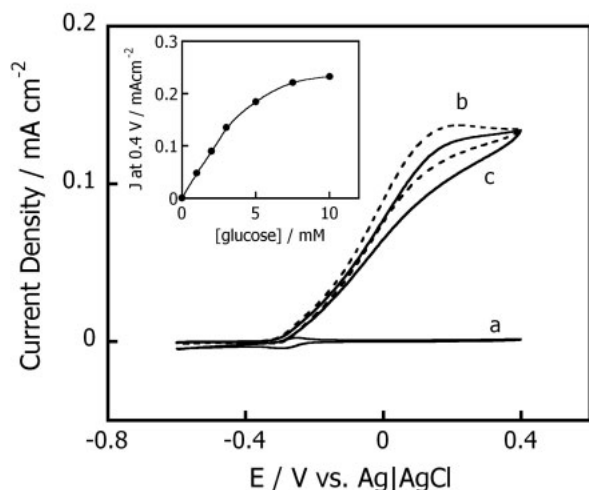


Fig. 3. (a) Cyclic voltammograms for an electrochemical cell containing a PLL-VK₃/Dp/GDH-modified GC electrode with a N₂-saturated pH 7.0 phosphate-buffered electrolyte solution at 37 °C. (b and c) Voltammograms for cells similar to that of Fig. 4(a) but with 3.0 mM NADH (b) or 3.0 mM glucose and 1.0 mM NAD⁺ (c) added to the electrolyte solutions. In all cases, the scan rate was 5 mV s⁻¹. The inset is a plot of the current density at 0.4 V versus the glucose concentration.

dehydrogenases, such as alcohol dehydrogenase, could replace GDH.

We have shown that addition of KB to a PAA-VK₃-modified electrode greatly increases the electrochemical activity of that electrode [10]. Figure. 4 shows that the addition of KB to the PLL-VK₃/DP/GDH-modified electrode produced approximately ten-fold larger current waves than that those found when KB was omitted (Compare the Y-axes of Fig. 3 and Fig. 4). Figure 4 insert shows the current density dependence on glucose concentration at 0.4 V in the presence of 1.0 mM NAD⁺. The effective surface area of the KB-modified electrode was estimated using the non-faradic current at -0.5 V and was found to be ca.46-fold larger than that of an unmodified GC electrode surface. The interactions between all components, i.e., the enzymes, the mediator, and the substrates, were not inhibited by the three-dimensional KB matrix. Although the shapes of the CVs suggest that an enzymatic reaction controlled the value of the catalytic current density, it could be further increased as high as 2 mA cm⁻² when the electrolyte solution was stirred (Fig. 4d).

We evaluated the effects of pH and temperature on the glucose oxidation performance of KB/PLL-VK₃/Dp/GDH-modified electrode (data not shown). The electrode functioned between pH 4.8 and 8.5 and showed maximal activity near pH 7. The electrode's performance improved with increasing temperature until reaching about 45 °C and then declined rapidly at higher temperatures. These results seem to directly reflect the enzymatic activity [27].

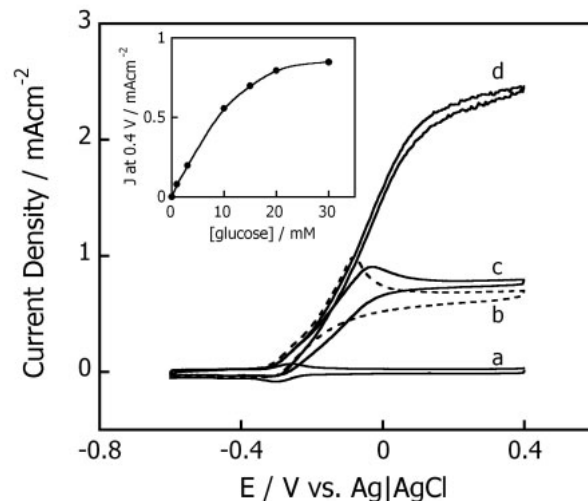


Fig. 4. (a) A cyclic voltammogram for a KB/PLL-VK₃/Dp/GDH-modified GC electrode in a N₂-saturated pH 7.0 phosphate-buffered electrolyte solution at 37 °C. (b-d) Cyclic voltammograms in the solution described in the legend of Fig. 4(a) but with 20 mM NADH (b), or 20 mM glucose, 1.0 mM NAD⁺ (c), or 30 mM glucose, 1.0 mM NAD⁺ (d). For (d), the electrolyte solution was stirred at 1000 rpm. In all cases the scan rate was 5 mV s⁻¹. The inset shows a plot of the current density at 0.4 V versus glucose concentration.

The stability of the modified-electrode when stored in a dry condition was evaluated daily by measuring the current density at 0 V (Fig. 5a). The electrode retained over 80% of its initial activity at day 7. However, when stored in a phosphate buffer at room temperature (Fig. 5b), the initial current density of 1.5 mAcm⁻² decreased to 0.3 mA cm⁻² within 2 days and then decreased more gradually during the next five days. Possibly, the electrode activity decay was caused by both enzyme deactivation and spatial disruption of the electron relay system (Fig. 1) that could, in turn, be caused by a swelling of the bilayer. Also a gradual desorption of mediators and enzymes from the swelled bilayer would cause the decay of electrode performance.

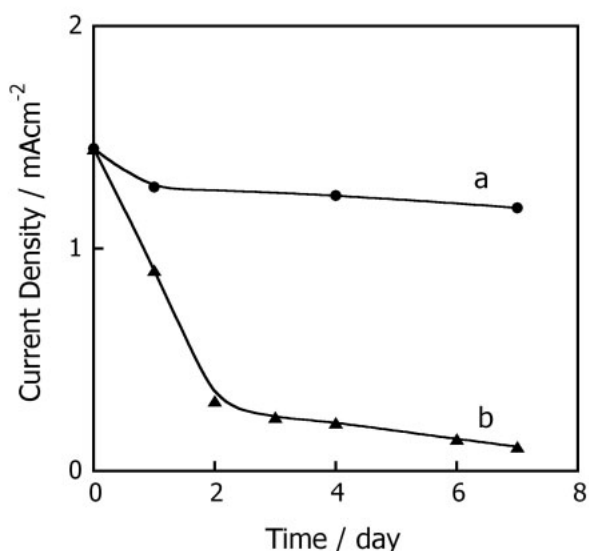


Fig. 5. Plots of the current density measured daily at 0 V in a N₂ saturated, 5.0 mM glucose, 1.0 mM NAD⁺ pH 7 phosphate-buffered electrolyte solution. The KB/PLL-VK₃/Dp/GDH-modified electrode that when not in use was (a) stored in air or (b) stored in the buffer solution (b).

3.2. Cell performance in a fluidic channel

Enzyme-based biofuel cells would be formatted into microfluidic systems as power sources for independent power-on-chip and implantable devices [2-5,7,14]. Such systems are also useful when evaluating the electrochemical stability of an experimental biofuel cell that is operating continuously, because the fuel flow rate, which can affect the cell's performance, can be regulated. We, therefore, constructed microfluidic-type cells (Fig. 2) containing an enzyme-modified Au anode and a PDMS-coated Pt or a Ag|AgCl cathode.

Figure 6 depicts the current-voltage profiles (A) and the power-voltage profiles (B) of these cells at a flow rate of 1.0 mL min⁻¹. Whether the fuel was N₂- (□) or air-saturated (Δ), a cell with a Ag|AgCl cathode, had a

maximum current density of 0.13 mAcm⁻² and a maximum power density of 20 μW cm⁻² at 0.2 V. However, the open circuit voltage (OCV) was somewhat greater for the cell with N₂-saturated fuel (0.37 V) than for the cell with air-saturated fuel (0.31 V). The dissolved oxygen will oxidize VK₃ and the enzymes [9], which, in turn, decreases the OCV value. Even so, dissolved oxygen seems not to have a decisive and detrimental effect on the redox reactions of Fig. 1. The glucose/O₂ biofuel cell's performance was evaluated when equipped with a KB/PLL-VK₃/Dp/GDH anode and a PDMS-coated Pt cathode (Fig. 6, ○). PDMS emulsion-coated electrodes selectively reduce oxygen [8]. To evaluate only the anode's performance, the area of the Pt cathode was ca. 10 times larger than that of the anode. The Pt cathode

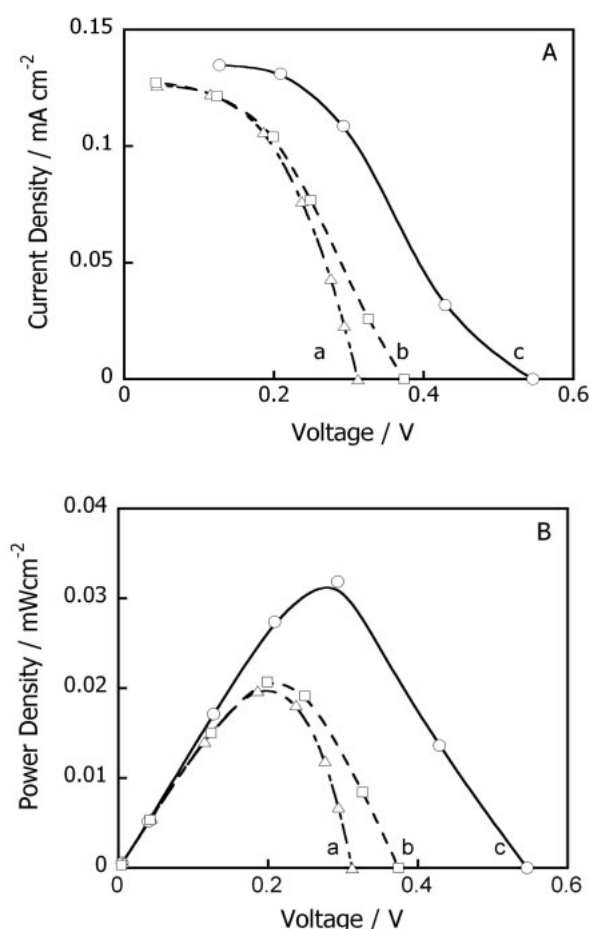


Fig. 6. (A) Current-voltage profiles and (B) power-voltage profiles for a fuel cell operating with a fuel flow rate of 1 mL min⁻¹ at 37 °C. The fuel was a pH 7 phosphate buffer containing 5.0 mM glucose and 1.0 mM NAD⁺. The anode was a KB/PLL-VK₃/Dp/GDH-coated Au electrode and the cathode was (a) a Ag|AgCl electrode (N₂-saturated fuel), (b) a Ag|AgCl electrode (air-saturated fuel) or (c) a PDMS-coated Pt (air-saturated fuel).

was placed upstream of the anode, to minimize the presence of contaminating O_2 in the anode's vicinity. For this system, the OCV is 0.55 V and the maximum power density was $32 \mu W cm^{-2}$ at 0.29 V. The maximum current density was again around $0.13 mA cm^{-2}$, indicating that the cell's performance was limited by reactions at the anode.

The cell's performance was affected by the flow rate of the fuel (Fig. 7). At a $100 k\Omega$ load, the discharge current density increased as the flow rate increased, which correlates with an increased delivery of fuel at the anode's surface. However, the direct relationship between the discharge current density and the flow rate could also be caused, in part or in whole, by a build-up of O_2 depletion layer in the anode's vicinity, which could occur effectively at lower flow rates. This possibility is supported by a numerical simulation that shows a growing O_2 depletion layer during pre-electrolysis of O_2 at a Pt cathode (data not shown). We are preparing a 3D microstructured cathode within the fluidic channel for effective pre-electrolysis elimination of O_2 .

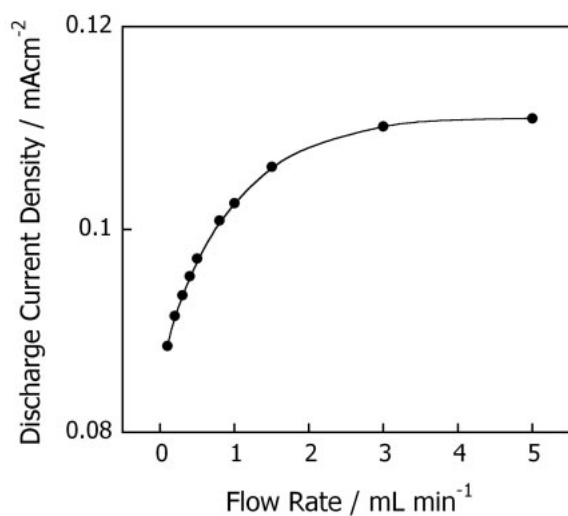


Fig. 7. A plot of the discharge current density vs. the fuel flow rate at $37^\circ C$ for a biofuel cell containing a KB/PLL-VK₃/Dp/GDH-modified anode and a PDMS-coated Pt cathode. The load was $100 k\Omega$. The fuel was an air-saturated pH 7.0 phosphate-buffered 1.0 mM NAD⁺, 5.0 mM glucose solution.

We tested the stabilities of the biofuel cells (each with one of the two cathodes) by continuously operating them with a flow rate of $1.0 mL min^{-1}$ and a $100 k\Omega$ load (Fig. 8). The values found for the discharge current densities at any given time for the two cells were essentially the same, indicating that reactions at the anodes controlled the cells' stabilities. During the first few hours of operation, the current increased, probably because the fuel penetrated into entire the bilayer. After peaking, the discharge current

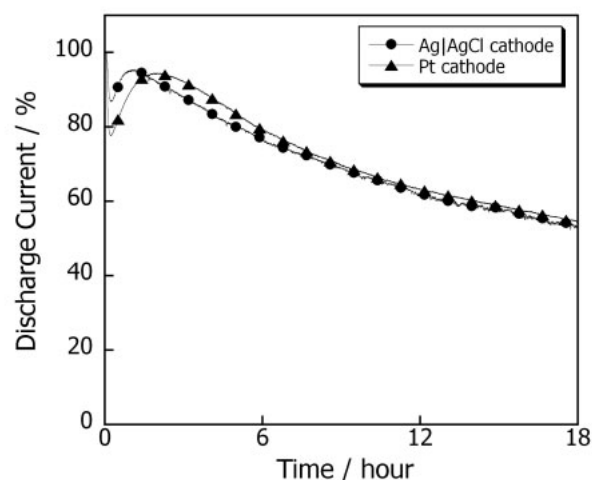


Fig. 8. Plots of the discharge current density ($R=100 k\Omega$) versus time of operation for biofuel cells containing a KB/PLL-VK₃/Dp/GDH anode and a Ag|AgCl cathode (●) or a PDMS-coated Pt cathode (▲), and an air-saturated pH 7.0 phosphate-buffered fuel containing 1.0 mM NAD⁺ and 5.0 mM glucose. Both cells were run, with a flow rate of $1.0 mL min^{-1}$.

slowly decreased. After 18 hours of continuous operation, for both cells, the discharge current density was ca. $0.05 mA cm^{-2}$, which was still larger than half of the initial value. As mentioned previously to explain the results, both gradual desorption of the enzymes and VK₃ and a partial functional degradation of the electron-relay system owing to bilayer swelling could cause the decrease in the discharge current densities. The cells' stabilities may be improved by optimizing the cross-linking of the PLL polymer and inhibiting swelling of the bilayer by physical means; e.g., lamination of the outer bilayer surface with an electrolyte-permeable film.

3.3. Oxygen elimination by upstream cathode

We constructed microfluidic fuel cells of the type shown in Fig. 9. Film electrodes were patterned on the surfaces of glass slides by photolithography and sputtering, which is a lift-off process. Both anode's (2.8 mm width, 1 mm long) and cathode's (2.8 mm width, 10 mm long) Au current collectors were modified by KB and enzymes. The gap between anode and cathode was 0.5 mm. The Ag|AgCl electrode was fabricated by coating a Pt film with Ag|AgCl ink (BAS Inc.) that was then cured at $80^\circ C$ for 2 h. A negative of the channel shape was prepared by thick photoresist (SU-8 2050, Microchem) by photolithography and transcribed to polydimethylsiloxane (PDMS; SYLPOT 184 W/C, Dow Corning Toray) slabs, so as to producing channels of 3 mm width and 0.1 mm or 1 mm height.

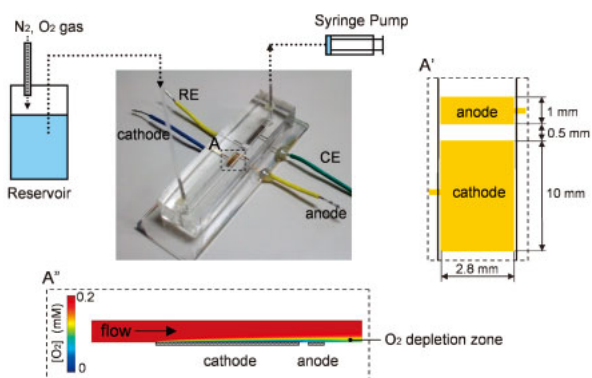


Fig. 9. Schematic illustration and photograph of microfluidic biofuel cell with (A') the close up top view of the electrodes and (A'') the cross-sectional view of a COMSOL simulation of an O_2 depletion layer forming along the channel.

Figure 10a shows linear sweep voltammograms (LSVs) of glucose anode (2.8 mm^2) in 0.3 mL min^{-1} (10 cm min^{-1}) flow of N_2 -bubbled phosphate buffer solution containing 10 mM glucose and 1.0 mM NAD^+ (\cdots), with a sigmoidal shape reaching $27 \mu\text{A}$ (ca. 1 mA cm^{-2}). The glucose oxidation currents obtained in air-saturated solution ($—$) and O_2 -saturated solution ($---$) were somewhat smaller than that in N_2 -bubbled solution, probably because the dissolved O_2 competes with electron relay at the PLL-VK₃/Dp/GDH/KB electrode. In addition to this short-term adverse effect

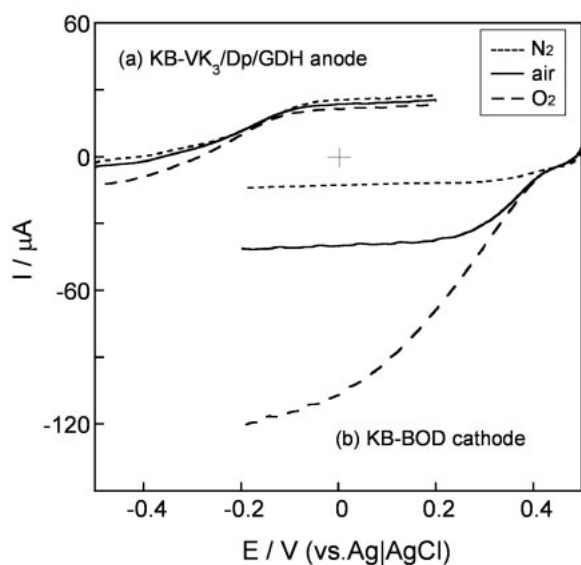


Fig. 10. LSVs of (a) anode and (b) cathode in N_2 -bubbled (\cdots), air-saturated ($—$), and O_2 -bubbled ($---$) 50 mM phosphate buffer (pH 7) containing 0.1 M NaCl , 1 mM NAD^+ and 10 mM glucose at room temperature, with a flow rate of 0.3 mL min^{-1} . Scan rate: 2 mV s^{-1} . Channel height: 1 mm .

of dissolved O_2 to anode, the irreversible oxidative degradation would occur during longer operation.

The LSVs of BOD-adsorbed KB electrode (10 mm long, 28 mm^2) are shown in Fig. 10b. In N_2 -bubbled solution (\cdots), only a small current was observed, but in air-saturated ($—$) and O_2 -bubbled solution ($---$), the O_2 reduction catalytic current clearly appeared at a potential more negative than 0.45 V . The starting potential of O_2 reduction current was about 0.2 V more positive than for the case with Pt electrode as the cathode. This was due to the direct electron transfer of BOD. The catalytic current reached $41 \mu\text{A}$ in air saturated solution and $120 \mu\text{A}$ in O_2 -bubbled solution.

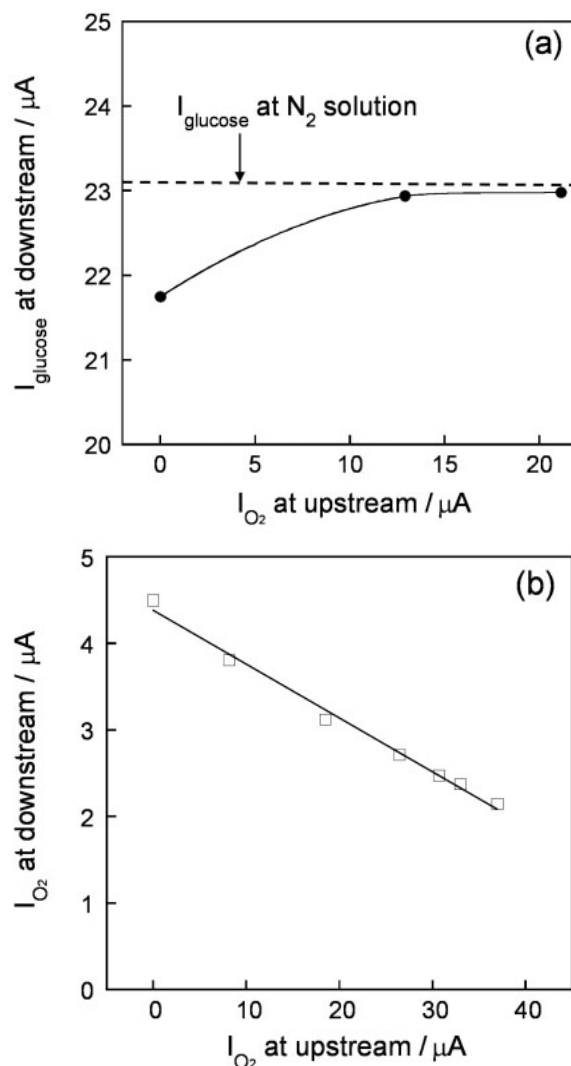


Fig. 11. (a) Glucose oxidation current of downstream glucose anode (I_{glucose} at downstream) vs. O_2 reduction current of upstream BOD cathode (I_{O_2} at upstream), and (b) O_2 reduction current of downstream BOD electrode (I_{O_2} at downstream) vs. O_2 reduction current of upstream BOD electrode (I_{O_2} at upstream), measured in the phosphate buffer (pH 7) containing 0.1 M NaCl , 10 mM glucose and 1 mM NAD^+ at room temperature, with a flow rate of 0.3 mL min^{-1} . Channel height: 1 mm .

The shape of LSV was not influenced by the additional presence of NAD^+ and glucose owing to the satisfying reaction selectivity of KB/BOD electrode to O_2 reduction. We have set the flow rate at 10 cm min^{-1} , where the diffusion layer of O_2 grows up to a few hundred μm but does not cover the 1 mm channel height, as theoretically discussed later.

As described above, we measured the polarization curve of the glucose electrode and O_2 electrode individually under operating conditions of the fuel cell by using the microfluidic biofuel cell system that internally contains a reference electrode and a counter electrode. In order to balance the current at anode and cathode, we set the area of the cathode (28 mm^2) ten times larger than the anode (2.8 mm^2). The combination of these electrodes is expected to show OCV of ca. 0.8 V and maximum current of ca. $25 \mu\text{A}$ (as limited by anode) in the air-saturated glucose solution. This expected cell performance could be obtained only if the anode is protected from O_2 without decreasing O_2 flux to the cathode.

With the aim of decreasing the O_2 flux to the anode as simulated in Fig. 9-A", we experimentally studied the effect of pre-reduction of O_2 at a cathode set upstream of the fluidic channel. Figure 11a shows the currents at the downstream glucose anode versus the O_2 reduction current at the upstream cathode. The glucose oxidation current (at 0V vs. Ag|AgCl) was successfully increased by the pre-reduction of O_2 by up to $23 \mu\text{A}$, nearly equal to that observed in the N_2 -bubbled solution (---), suggesting that the degree of decrease in O_2 flux in the vicinity of the anode was sufficient to prevent the adverse reaction of O_2 . The pre-reduction should become more significant at lower glucose concentration or higher O_2 concentration due to the relatively larger flux of competitive O_2 . The O_2 flux downstream was estimated by experiments using the KB/BOD electrode for both upstream and even downstream (Fig. 11b). The O_2 reduction current (at -0.4 V vs. Ag|AgCl) at the downstream KB/BOD electrode (i_{O_2} at downstream) decreased linearly with increasing pre-reduction current (i_{O_2} at upstream). This linear relationship can be expressed as the equation,

$$i_{\text{downstream}} = i_{\text{downstream}}^0 - N \cdot i_{\text{upstream}} \quad (1)$$

where $i_{\text{downstream}}^0$ is the current at the downstream electrode when $i_{\text{upstream}} = 0$, and N is the efficiency of O_2 elimination estimated as 0.065 from the decay of the plot. The experimental N value (0.065) is unfortunately inferior to the theoretical one ($N_{th} = 0.13$) calculated by the equation for the channel flow electrode system, probably because of unknown factors affecting N : eg., the thickness (several tens of μm) and roughness of the KB electrodes. The N_{th} is the function of only electrode configuration, and suggests that a higher N_{th} would be obtained by a narrower electrode gap and smaller upstream cathode, while the small

cathode has the disadvantage for generating larger power.

By connecting enzymatic anode and cathode through external resistance, biofuel cell performance was evaluated for 0.3 mL min^{-1} . Figure 12a shows the cell performance (V-I curve) in an air-saturated solution with an open circuit voltage (V_{oc}) of around 0.8 V and maximum current (I_{max}) of over $20 \mu\text{A}$. This is in agreement with the prediction from performance of each anode and cathode. The V-I curve obtained with the upstream-cathode cell (\bullet) was bigger than that with the downstream-cathode cell (\blacktriangle), especially in the higher current region. The I_{max} increased 10 % by placing the cathode upstream, mainly reflecting the improved anode as judged from the analogy between the shape of the V-I curve of the cell (—) and the E-I curve of the anode (\cdots). The E-I curve of the cathode (---) was also somewhat changed, indicating the consumption of O_2 at the upstream anode by the adverse reaction with enzymes and mediators. Another separate experiment with an O_2 -bubbled solution brought smaller I_{max} (ca. $20 \mu\text{A}$) due to the larger O_2 flux to the upstream anode, which was improved 15 %

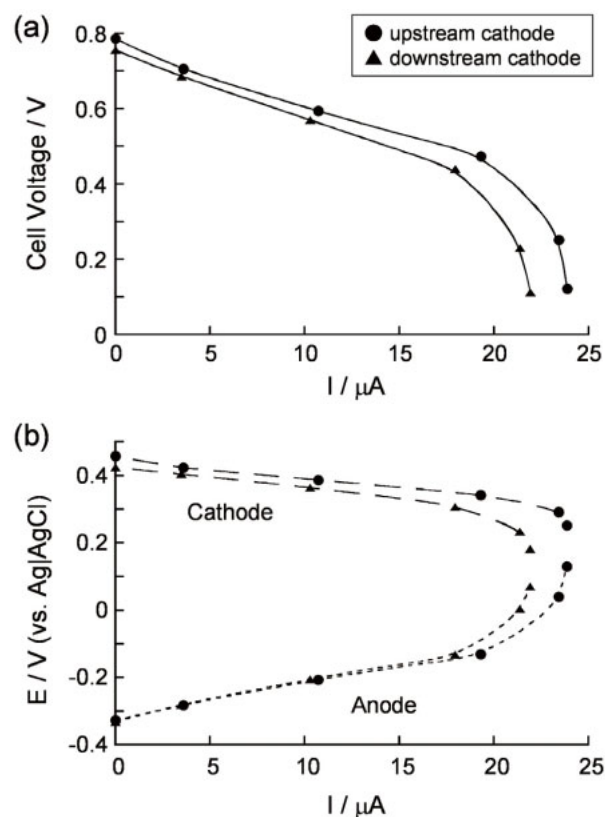


Fig. 12. (a) V-I curve of microfluidic biofuel cell (—), and (b) E-I curves of anode (\cdots) and cathode (---) operating under air-saturated phosphate buffer (pH 7) containing 0.1 M NaCl, 10 mM glucose and 1 mM NAD^+ at room temperature, with a flow rate of 0.3 mL min^{-1} . The cells were operated with upstream cathode (\bullet) or downstream cathode (\blacktriangle). Channel height: 1 mm.

by pre-reduction of O₂ at the upstream cathode. These results have proven that the cell design with upstream cathode is effective in protecting the anode from the oxidative environment and consequently improving cell performance.

We also studied the performance of microfluidic biofuel cells having electrodes on both bottom and upper walls of the channel. These were constructed by sandwiching a silicone rubber spacer of 0.1 mm or 1 mm thickness between two electrode-patterned glass slides. Both glass slides have a set of upstream cathode and downstream anode. The I_{max} of the 1 mm-height cell (44 μA) was almost twice that for the case of a single set of electrodes. This result directly corresponds to the increased electrode area. In contrast, the I_{max} of 0.1 mm-height cell (▲) composed of two sets of electrodes became rather small mainly because of depletion of O₂ in the narrower flow channel, as presumed from the degraded cathodic I-E curve. Theoretically, at the maximum diffusional flux (*c*=0 at the electrode surface), the thickness of the diffusion boundary layer δ (cm) formed on the electrode within a tube-shaped channel is expressed as,

$$\delta = \frac{1}{0.67} \left(\frac{DRx}{v_0} \right)^{1/3} \quad (2)$$

where *D* is the diffusion coefficient (cm² s⁻¹), *R* is the radius of the tube, *x* is the distance measured downstream from the leading edge of the electrode (cm) and *v*₀ is the maximum velocity at the axis of the tube (*r*=0) (cm s⁻¹). From Eq.(2), the thickness of the O₂ depletion layer under the flow condition of 10 cm min⁻¹ (0.3 mL min⁻¹) is calculated to be about several hundred μm at a position 1 mm-downstream from the leading edge of the cathode, which can fully cover the 0.1 mm-height fluidic channel and lower cell performance. On the other hand, from the viewpoint of the “volume density”, the 0.1 mm-height narrower cell is superior to the 1 mm-height cell; the volume density of I_{max} and P_{max} of the 0.1 mm-height cell was 3.8 times and 2 times, respectively, as large as those of the 1 mm-height cell. The optimum efficient operation with the highest density of output would be at the flow condition forming depletion layer comparable to the channel height.

4. Conclusion

PLL-VK₃ was a mediator of Dp/GDH-catalyzed glucose oxidation. Other enzyme bilayers could be developed that would accommodate a different NAD⁺-dependent enzymes, and, thus, when any one such bilayer is a part of an anode in a biofuel cell, the cell could use a different fuel. We used fluidic cells with controlled fuel flow rates to evaluate the properties (e.g., stability) of a KB/PLL-VK₃/Dp/GDH electrode.

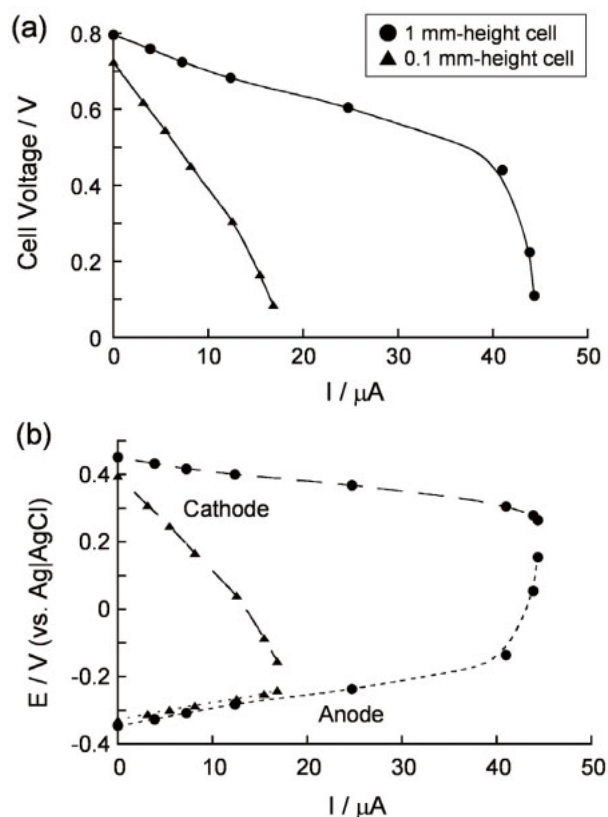


Fig. 13. (a) V-I curves of sandwich type microfluidic biofuel cell (—), and (b) E-I curves of anode (···) and cathode (---) operating under air-saturated phosphate buffer (pH 7) containing 0.1 M NaCl, 10 mM glucose and 1 mM NAD⁺ at room temperature, with a mean flow rate of 10 cm min⁻¹. Channel height: 1 mm (●) and 0.1 mm (▲).

The observed decay of electrode activity during the continued operation of the cells is probably partially caused by swelling of the bilayer. Lamination with an electrolyte-permeable film might prevent excessive swelling. Oxidative degradation of the enzymes and the mediator would be a serious problem during longer periods of operation. The upstream cathode successfully reduced the O₂ flux to the anode, and consequently improved the glucose oxidation performance. The maximum cell current with the upstream-cathode cell was about 10 % higher than that with the downstream-cathode cell. It was experimentally demonstrated that, we need to take into account the depletion of fuel and oxidant within the channel that depends on the channel height and flow rate in addition to the electrode configuration. One of the optimum operating conditions would be when the flow forming depletion layer is comparable to the channel height. The active O₂ supply from external air through the channel wall should be effective in improving the cell performance. In such an O₂-concentrated condition, the cell construction with upstream cathode would become more significant to maintain anode's performance.

Acknowledgements

We acknowledge the support of Tohoku University Global COE Program "Nano-Biomedical Engineering Education and Research Network Centre".

References

- [1] Willner B and Willner I. Reconstituted Redox Enzymes on Electrodes: From Fundamental Understanding of Electron Transfer at Functionalized Electrode Interfaces to Biosensor and Biofuel Cell Applications. In: *Bioelectronics*, edited by Willner I and Katz E, Wiley-VCH, Weinheim, 35-93, 2005.
- [2] Mano N, Mao F, and Heller A. Characteristics of a miniature compartment-less glucose-O₂ biofuel cell and its operation in a living plant. *J Am Chem Soc* **125**, 6588-6594, 2003.
- [3] Heller A. Miniature biofuel cells. *Phys Chem Chem Phys* **6**, 209-216, 2004.
- [4] Heller A. Integrated medical feedback systems for drug delivery. *AIChE Journal* **51**, 1054-1066, 2005.
- [5] Heller A. Potentially implantable miniature batteries. *Anal Bioanal Chem* **385**, 469-473, 2006.
- [6] Katz E, Filanovsky B, and Willner I. A biofuel cell based on two immiscible solvents and glucose oxidase and microperoxidase-11 monolayer-functionalized electrodes. *New J Chem*, 481-487, 1999.
- [7] Katz E, Buckmann AF, and Willner I. Self-powered enzyme-based biosensors. *J Am Chem Soc* **123**, 10752-10753, 2001.
- [8] Tamaki T and Yamaguchi T. High-surface-area three-dimensional biofuel cell electrode using redox-polymer-grafted carbon. *Int Eng Chem Res* **45**, 3050-3058, 2006.
- [9] Tsujimura S, Kano K, and Ikeda T. Glucose/O₂ biofuel cell operating at physiological conditions. *Electrochemistry* **70**, 940-942, 2002.
- [10] Sato F, Togo M, Islam MK, Matsue T, Kosuge J, Fukasaku N, Kurosawa S, and Nishizawa M. Enzyme-based glucose fuel cell using vitamin K₃-immobilized polymer as an electron mediator. *Electrochem Commun* **7**, 643-647, 2005.
- [11] Akers NL, Moore CM, and Minter SD. Development of alcohol/O₂ biofuel cells using salt-extracted tetrabutylammonium bromide/Nafion membranes to immobilize dehydrogenase enzymes. *Electrochim Acta* **50**, 2521-2525, 2005.
- [12] Moore CM, Minter SD, and Martin RS. Microchip-based ethanol/oxygen biofuel cell. *Lab Chip* **5**, 218-225, 2005.
- [13] Palmore GTR, Bertschy H, Bergens SH, and Whitesides GM. A methanol/dioxygen biofuel cell that uses NAD⁺-dependent dehydrogenase as catalysts: application of an electro-enzymatic method to regenerate nicotiamide adenine dinucleotide at low overpotentials. *J Electroanal Chem* **443**, 155-161, 1998.
- [14] Barton SC, Gallaway J, and Atanassov P. Enzymatic biofuel cell for implantable and microscale devices. *Chem Rev* **104**, 4867-4886, 2004.
- [15] Kano K and Ikeda T. Fundamentals and practices of mediated bioelectrocatalysis. *Anal Sci* **16**, 1013-1021, 2000.
- [16] Kano K and Ikeda T. Bioelectrocatalysis, powerful means of connecting electrochemistry to biochemistry and biotechnology. *Electrochemistry* **71**, 86-99, 2003.
- [17] Tsujimura S, Kano K, and Ikeda T. Bilirubin oxidase in multiple layers catalyzes four-electron reduction of dioxygen to water without redox mediators. *J Electroanal Chem* **576**, 113-120, 2005.
- [18] Tsujimura S, Nakagawa T, Kano K, and Ikeda T. Kinetic study of direct bioelectrocatalysis of dioxygen reduction with bilirubin oxidase at carbon electrodes. *Electrochemistry* **72**, 437-439, 2004.
- [19] Sato A, Kano K, and Ikeda T. Diaphorase/naphthoquinone derivative-modified electrode as an anode for diffusion-controlled oxidation of NADH in electrochemical cells. *Chem Lett* **32**, 880-881, 2003.
- [20] Ogino Y, Takagi K, Kano K, and Ikeda T. Reactions between diaphorase and quinine compounds in bioelectrocatalytic redox reactions of NADH and NAD⁺. *J Electroanal Chem* **396**, 517-524, 1995.
- [21] Sammoura F, Lee KB, and Lin L. Water-activated disposable and long shelf life microbatteries. *Sens Act A* **111**, 79-86, 2004.
- [22] Lee KB. Urine-activated paper batteries for biosystems. *J Micromech Microeng* **15**, S210-S214 2005.
- [23] Ferrigno R, Strook AD, Clark TD, Mayer M and Whitesides GM. Membraneless vanadium redox fuel cell using laminar flow. *J Am Chem Soc* **124**, 12930-12931, 2002.
- [24] Choban ER, Markoski LJ, Wieckowski A, and Kenis PJA. Microfluidic fuel cell based on laminar flow. *J Power Sources* **128**, 54-60, 2004.
- [25] Jayashree RS, Gancs L, Choban ER, Primak A, Natarajan D, Markoski LJ, and Kenis PJA. Air-breathing flow-based microfluidic fuel cell. *J Am Chem Soc* **127**, 16758-16759, 2005.
- [26] Mizutani F, Sato Y, Hirata Y, and Iijima S. Interference-free, amperometric measurement of urea in biological samples using an electrode coated with tri-enzyme/polydimethylsiloxane-bilayer membrane. *Anal Chim Acta* **441**, 175-181, 2001.
- [27] <http://www.toyobo.co.jp/e/seihin/xr/enzyme/prod uct.html>
- [28] Tatsumi H, Nakase H, Kano K, and Ikeda T. Mechanic study of the autoxidation of reduced flavin and quinine compounds. *J Electroanal Chem* **443**, 236-242, 1998.